Heterojunction Photovoltaics Using Printed Colloidal Quantum Dots as a Photosensitive Layer

ARTICLE *in* NANO LETTERS · FEBRUARY 2009

Impact Factor: 13.59 · DOI: 10.1021/nl803760j · Source: PubMed

5 AUTHORS, INCLUDING:

Alexi Arango
Mount Holyoke College
16 PUBLICATIONS **776** CITATIONS

SEE PROFILE

NANO LETTERS

Letter

Heterojunction Photovoltaics Using Printed Colloidal Quantum Dots as a Photosensitive Layer

Alexi C. Arango, David C. Oertel, Youfeng Xu, Moungi G. Bawendi, and Vladimir Bulovic#

Nano Lett., **2009**, 9 (2), 860-863• DOI: 10.1021/nl803760j • Publication Date (Web): 22 January 2009

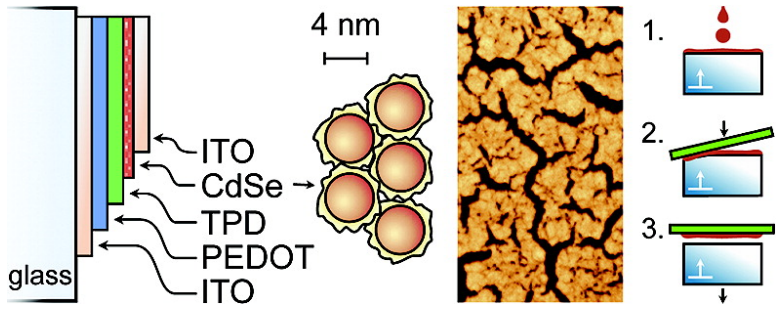

More About This Article

Additional resources and features associated with this article are available within the HTML version:

- Supporting Information
- Access to high resolution figures
- Links to articles and content related to this article
- Copyright permission to reproduce figures and/or text from this article

View the Full Text HTML

NANO LETTERS

2009
Vol. 9, No. 2
860-863

Heterojunction Photovoltaics Using Printed Colloidal Quantum Dots as a Photosensitive Layer

Alexi C. Arango,[†] David C. Oertel,[‡] Youfeng Xu,[†] Moungi G. Bawendi,[‡] and Vladimir Bulović*[,†]

Department of Electrical Engineering and Computer Science and Department of Chemistry, Massachusetts Institute of Technology, Cambridge, Massachusetts 02139

Received December 12, 2008; Revised Manuscript Received January 15, 2009

ABSTRACT

We demonstrate a bilayer photovoltaic device consisting of a heterojunction between colloidal cadmium selenide (CdSe) quantum dots (QDs) and a wide band gap organic hole-transporting thin film of *N*,*N*′-diphenyl-*N*,*N*′-bis(3-methylphenyl)[1,1′-biphenyl]-4,4′-diamine (TPD) molecules. The active light-absorbing film of QDs is nondestructively printed onto TPD using microcontact stamping. Indium−tin−oxide (ITO) provides the top contact. The resulting device structure can accommodate different size QDs, produces an exceptionally large open circuit voltage (0.8 V) for an architecture with symmetric electrodes, and yields an internal quantum efficiency of 10% at the first QD absorption peak.

Colloidally synthesized quantum dot (QD) systems offer distinct optical and electronic properties that are not easily attained by other nanostructured semiconductors, such as highly saturated emission in QD light-emitting diodes,[1] access to infrared radiation in QD photodetectors,[2,3] and the prospect of optically optimized solar cell structures. The prevailing deposition method for colloidal QD systems is spin casting,[4] which introduces limitations such as solvent incompatibility with underlying films and the inability to pattern side-by-side pixels for multispectral photodetector arrays. The alternative deposition method of drop casting is applicable to the fabrication of lateral QD devices (such as photoconductors[5] and transistors [6]), but resulting films are generally of nonuniform thickness and unsuitable for vertical heterojunction structures.

In this Letter, we describe a QD-based photovoltaic architecture that employs two innovative device fabrication methods (Figure 1). First, a thin QD film (∼20 nm) is deposited onto an organic hole transport layer using a nondestructive microcontact printing method.[7] The QD film consists of colloidally grown cadmium selenide (CdSe) nanocrystals, which serve as the principle photoactive species. The organic film consists of *N*,*N*′-diphenyl-*N*,*N*′-bis(3-methylphenyl)[1,1′-biphenyl]-4,4′-diamine (TPD), which serves as a transparent hole-transport window layer. Second, a thin film of indium−tin−oxide (ITO) is nondestructively sputter-deposited onto the QD layer as a transparent top

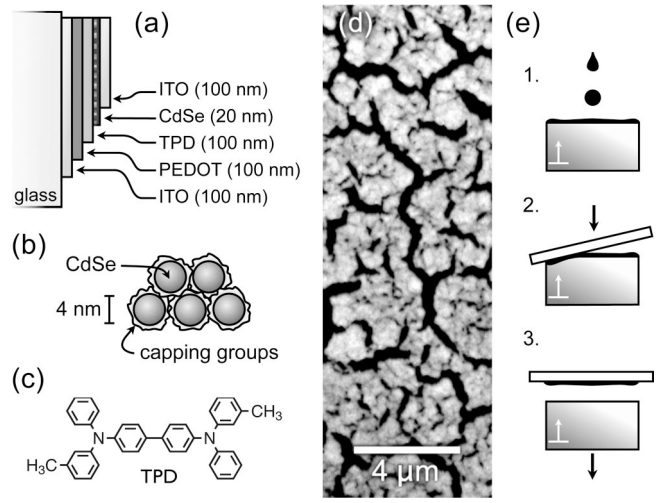

Figure 1. Diagram of (a) ITO/PEDOT/TPD/CdSe/ITO device structure, (b) CdSe QDs with organic capping groups, and (c) molecular structure of TPD. An atomic force microscopy image of the printed CdSe film is shown in (d). A diagram of the printing process is shown in (e): the CdSe suspension is spin cast onto a PDMS stamp and allowed to dry (1), the TPD-coated substrate and stamp are pressed together (2), and the substrate and stamp are separated (3).

electrode. The transparency in the visible part of the spectrum of the ITO top electrode ensures that the optical field intensity near the top electrode interface—where the QDs are located—is not suppressed. With the nondestructive QD printing process, a distinct planar heterojunction is formed between the neat QD film and the underlying TPD. The thickness of the QD film is kept as thin as possible in order to limit losses

* Corresponding author, bulovic@mit.edu.
[†] Department of Electrical Engineering and Computer Science.
[‡] Department of Chemistry.

10.1021/nl803760j CCC: $40.75
Published on Web 01/22/2009

associated with exciton diffusion or carrier transport across the QD's insulating capping groups. The resulting device structure is free of a low work function metallic contact that can easily oxidize and lead to poor device stability.

The device structure is shown in Figure 1a and consists of the following sequence of films and thicknesses: ITO/poly(3,4-ethylenedioxythiophene) poly(styrenesulfonate) (PEDOT:PSS) (100 nm)/TPD (100 nm)/CdSe/ITO (100 nm). PEDOT:PSS (Baytron P VP CH 8000) is spin cast onto a 0.5 × 0.5 in.^{2} glass substrate with prepatterned ITO electrodes. The TPD (H. W. Sands) layer is evaporated at a rate of 0.1 nm/s, which is followed by print deposition of the CdSe layer in a nitrogen-atmosphere glovebox. The elastomeric stamps used for QD printing are made by casting poly(dimethylsiloxane) (PDMS) that is cured at 60 °C for 2 h to form an optically smooth conformable surface, and then sectioned into 1 cm^2 stamps. Sixty microliters of a chloroform solution containing CdSe QDs, capped with oleate groups and synthesized according to Jarosz et al.,[5] is dispensed on the stamp, spun at 3000 rpm, and allowed to dry (Figure 1e), forming a thin QD film coating on top of the stamp. The coated stamp is then pressed against the device stack, making contact first at one edge to minimize air pockets trapped between the stamp and the substrate. The stamp and substrate are then immediately separated, leaving the CdSe film adhered to the TPD. The top ITO contact is rf sputter deposited through a shadow mask to generate an array of patterned electrodes. ITO sputtering is performed at room temperature at a rate of 0.01 nm/s for the first 20 nm in order to minimize damage to the underlying CdSe and TPD films. The remaining 80 nm of the ITO film is grown at 0.07 nm/s. The final device area of 1.21 mm^2 is defined by the overlap between the top and bottom ITO electrodes.

Current−voltage ($i-\upsilon$) characteristics of the finished devices are measured in a nitrogen atmosphere glovebox with a source-meter (Keithley 6487). The light response is measured under illumination from a green LED (Lamina, Light Engine) with a peak wavelength of $\lambda = 532$ nm and light output of approximately 78 mW/cm^2 at 2 A. The photoaction spectra are measured with a lock-in amplifier (Stanford Research Systems SR830), under illumination from monochromatic light generated by a xenon arc lamp coupled to a monochromator (Acton 300i) and chopped at 44 Hz. A calibrated silicon photodiode (Newport 818-UV) is used to measure the incident monochromatic light intensity. Transmittance and reflectance spectra of the entire device stack are measured with an Aquila Instruments nkd-8000.

The quantum efficiency (QE) at zero bias is plotted in Figure 2, along with the device absorption for QDs with diameters of 4, 5, and 8 nm, corresponding to first transition energies (E_1) of 2.2, 2.1, and 1.9 eV, respectively. The photocurrent spectrum follows the QD absorption profile below 3 eV, yet is dominated by TPD absorption and photoresponse above 3 eV. The magnitude of the quantum efficiency at the first absorption peak of the QDs is low (∼0.3%), in part due to limited light absorption (∼3%) in the very thin QD films. From the transmission and reflection

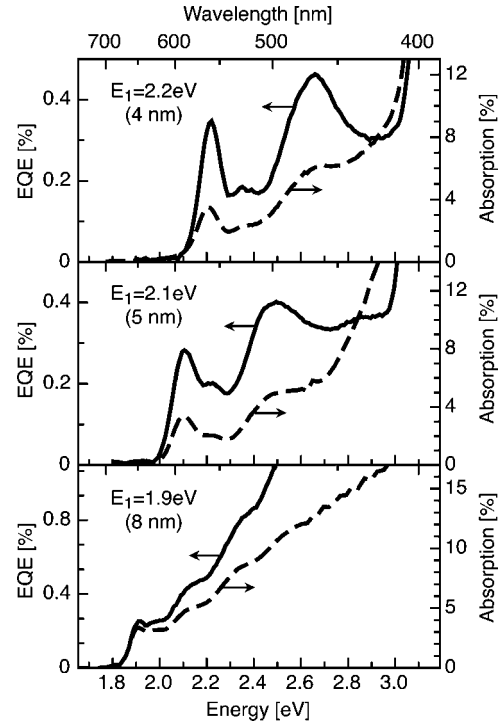

Figure 2. Quantum efficiency versus incident photon energy (solid line) and absorption spectra (dotted line) for ITO/PEDOT/TPD/CdSe/ITO devices with QD diameters of 4, 5, and 8 nm.

spectra of the completed devices, we can extrapolate the internal quantum efficiency to be approximately 9.9% at the first absorption peak for the device with $E_1 = 2.2$ eV, 8.4% for the device with $E_1 = 2.1$ eV, and 7.6% for the device with $E_1 = 1.9$ eV. The observed decrease in IQE with band gap may be due to a decrease in electron transfer efficiency at the QD/ITO interface. The energy offset between the electron affinity of the QDs and the work function of ITO is approximately 0.2, 0.1, and −0.1 eV for $E_1 = 2.2$ eV, $E_1 = 2.1$ eV, and $E_1 = 1.9$ eV, respectively. However, we note that none of the devices has been optimized and therefore may not reflect the true trend with band gap.

Atomic force microscopy images of the surface of the QD film printed on top of TPD (Figure 1d) indicate cracking due to tensile stress in the plane of the film during the drying process. The cracked regions are completely void of QDs, leaving the underlying TPD film exposed to the top electrode. However, the partial coverage of the QD film does not appear to compromise the film's ability to photogenerate charge, despite the fact that incomplete films in photovoltaic devices are typically rendered useless by parasitic shunting.

The current−voltage characteristics for both ITO/PEDOT/TPD/QD/ITO and a control device without QDs (ITO/PEDOT/TPD/ITO), shown in Figure 3, help explain why voids in the QD film do not interrupt photocurrent generation. In the control structure without QDs, hole injection in forward bias at the PEDOT electrode can support higher current densities than hole injection in reverse bias at the top ITO electrode. With the addition of the QD layer, the forward bias current increases, which can be attributed to a new conduction pathway: electron injection from ITO to the

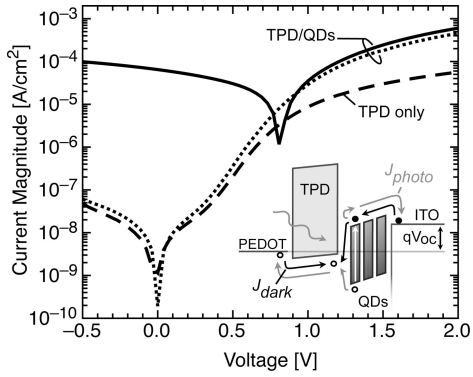

Figure 3. Semilogarithmic plot of the $i-v$ characteristics in the dark (dotted line) and under illumination at wavelength $\lambda = 532$ nm, 78 mW/cm^2 (solid line) for ITO/PEDOT/TPD/QD/ITO (QD diameter of 4 nm) and $i-v$ characteristics for ITO/PEDOT/TPD/ITO (dashed line) in the dark. No light response at 532 nm is observed for the device structure which does not contain QDs. The inset schematic illustrates the two most prominent current flow pathways at a bias point of V_{OC}. Under forward bias, current flow in the dark (J_{dark}, drawn in black) is due to electron injection at the ITO electrode, hole injection at the PEDOT electrode and charge recombination at the junction interface. Under illumination, photocurrent flow (J_{photo}, drawn in gray) occurs by absorption and charge excitation in the QDs, followed by hole transfer to TPD, electron transfer to the ITO electrode, and hole migration toward the PEDOT electrode. In the absence of additional current pathways, J_{dark} and J_{photo} must be equal and opposite at V_{OC}.

QDs and recombination with holes across the heterojunction interface (see inset, Figure 3). Under illumination, charge generated in the QD film contributes to photocurrent (J_{photo}) in both reverse bias and forward bias, as expected based on the favorable alignment of the energy bands. However, one would expect the presence of voids in the QD film to disrupt charge generation because a parasitic recombination pathway should be available for photoexcited holes to transfer from the QDs to the TPD and back to the top ITO electrode, resulting in a loss of photogenerated charge. The relative insignificance of this recombination pathway implies that coupling between holes in the TPD and conducting states in the ITO is inefficient. This result is consistent with the observation of a hole-blocking contact between the ITO and TPD by Shen et al.[8]

The V_{OC} of 0.8 V is significantly higher than expected considering the small work function difference of 0.4 eV between the PEDOT (5.2 eV) and ITO (4.8 eV) electrodes or the energy offset between the electron affinity of the QDs (4.6 eV) and the ionization potential of TPD (5.4 eV), which amounts to an offset of 0.8 eV. Neither a Schottky device model, where the maximum V_{OC} is determined by the difference between electrode work functions,[9,10] nor a donor/acceptor model, where the maximum V_{OC} is determined by the difference between the electron affinity of the acceptor and the ionization potential of the donor,[11] can fully account for the observed V_{OC}. Furthermore, it is unlikely that the V_{OC} of 0.8 V is fully saturated given the low photocurrent densities obtained at short circuit.

The high V_{OC} can be ascribed to two factors: low J_{dark} due to the rectifying TPD/ITO heterojunction, and diffusion of photoexcited carriers away from the heterojunction interface.[12,13] However, a large diffusion current requires a buildup of space charge at the heterojunction interface, which can only be accomplished if rates of recombination are much lower than rates of charge extraction. For example, in our structure, hole transfer at the QD/TPD heterojunction and electron transfer at the QD/ITO heterojunction increase charge build-up (and add to J_{photo}), while recombination at these interfaces decreases charge buildup (and reduces J_{photo}). Therefore, the large V_{OC} must be associated with reduced interfacial recombination relative to rates of charge extraction.[14]

The physical mechanism responsible for the favorable balance of charge extraction and recombination rates could be the presence of insulating organic capping groups on the QDs, which serve to passivate the QD surface and suppress parasitic recombination processes. In particular, the spatial separation between electrons and holes confined at the TPD/QD or QD/ITO interface reduces the wave function overlap between opposite charge across the heterojunction, resulting in less interfacial recombination, higher carrier concentrations, higher J_{photo} and higher V_{OC}.

The bilayered heterojunction photovoltaic structure presented in this study constitutes an initial attempt to reveal the underlying physics responsible for charge generation in nanostructured photovoltaics containing colloidal QDs. The structure is particularly tolerant to voids in the photoactive layer and therefore convenient for the study of thin photosensitive films. The ability to generate a large open-circuit voltage without the need for a low work function electrode should lead to improved reliability in solar applications. Indeed, devices stored in a nitrogen glovebox exhibit a remarkable shelf life, with no decay in short-circuit current and only a 10% decay in open-circuit voltage after more than a year. In order to increase device efficiency, thicker QD films with improved conductivity and greater absorption must be implemented. Because the QD film is printed and the overall device structure is transparent, advanced multilayered photovoltaic architectures should be achievable, such as stacked solar cells. Finally, the ability to define the spectral response of the device by choosing the QD size is useful for both stacked solar cells and multispectral photodetector arrays.

In conclusion, the organic/QD bilayer structure presented here is shown to generate photocurrent from absorption in the QD film and to accommodate different size QDs. Physical voids in the QD film are observed, but do not interrupt the generation of photocurrent or photovoltage. The high V_{OC} and negligible shunting are attributed to the hole-blocking character of the top ITO contact and low rates of interfacial recombination. Further development will require the use of thicker QD films in order to boost device absorption.

Acknowledgment. The authors thank LeeAnn Kim for lending her expertise in the microcontact stamping of QD films. This research was supported in part by the U.S. Army through the Institute for Soldier Nanotechnologies, under Contract W911NF-07-D-0004 with the U.S. Army Research Office and made use of the Shared Experimental Facilities supported in part by the MRSEC Program of the National

Science Foundation under award number DMR 02-13282. D.C.O. was supported by the Fannie and John Hertz Foundation.

References

(1) Coe, S.; Woo, W.; Bawendi, M.; Bulovic, V. *Nature* **2002**, *420*, 800–803.
(2) Rogalski, A. J. *Appl. Phys.* **2003**, *93*, 4355–4391.
(3) Maria, A.; Cyr, P. W.; Klern, E. J. D.; Levina, L.; Sargent, E. H. *Appl. Phys. Lett.* **2005**, *87*, 213112.
(4) Oertel, D. C.; Bawendi, M. G.; Arango, A. C.; Bulovic, V. *Appl. Phys. Lett.* **2005**, *87*, 213505.
(5) Jarosz, M. V.; Porter, V. J.; Fisher, B. R.; Kastner, M. A.; Bawendi, M. G. *Phys. Rev. B* **2004**, *70*, 195327.
(6) Mentzel, T. S.; Porter, V. J.; Geyer, S.; MacLean, K.; Bawendi, M. G.; Kastner, M. A. *Phys. Rev. B* **2008**, *77*, 075316.
(7) Kim, L.; Anikeeva, P. O.; Coe-Sullivan, S. A.; Steckel, J. S.; Bawendi, M. G.; Bulovic, V. *Nano Lett.* **2008**, *8*, 4513–4517.
(8) Shen, Y. L.; Jacobs, D. B.; Malliaras, G. G.; Koley, G.; Spencer, M. G.; Ioannidis, A. *Adv. Mater.* **2001**, *13*, 1234–1238.
(9) Luther, J. M.; Law, M.; Beard, M. C.; Song, Q.; Reese, M. O.; Ellingson, R. J.; Nozik, A. J. *Nano Lett.* **2008**, *8*, 3488–3492.
(10) Johnston, K. W.; Pattantyus-Abraham, A. G.; Clifford, J. P.; Myrskog, S. H.; Hoogland, S.; Shukla, H.; Klem, E. J. D.; Levina, L.; Sargent, E. H. *Appl. Phys. Lett.* **2008**, *92*, 122111.
(11) Rand, B. P.; Burk, D. P.; Forrest, S. R. *Phys. Rev. B* **2007**, *75*, 115327.
(12) Ramsdale, C.; Barker, J.; Arias, A.; MacKenzie, J.; Friend, R.; Greenham, N. *J. Appl. Phys.* **2002**, *92*, 4266–4270.
(13) Gregg, B. A. *J. Phys. Chem. B* **2003**, *107*, 4688–4698.
(14) Nelson, J.; Kirkpatrick, J.; Ravirajan, P. *Phys. Rev. B* **2004**, *69*, 035337.

NL803760J